Characterization of Fault Size in Bearings

Matan Mendelovich [1], Yitschak Sanders [1], Gideon Kogan [1], Mor Battat [1], Dr. Renata Klein [2], and Prof. Jacob Bortman [1]

[1] *Laboratory for Health, Department of Mechanical Engineering, Ben-Gurion University of the Negev, P.O. Box 653, Beer Sheva 84105, Israel*

matan.mendelovich@gmail.com
jitschaks@gmail.com
ggkogan@gmail.com
morbat@post.bgu.ac.il
jacbort@gmail.com

[2]*R.K. Diagnostics, Gilon, P.O.B. 101, D.N. Misgav 20103, Israel*
Renata.Klein@RKDiagnostics.co.il

ABSTRACT

Bearings are important components in rotating machines. An initial small damage in the bearing may cause a fast degradation, which may lead to the machine breakdown. The health condition of bearings can be monitored using proven vibro-acoustic methods effective for detecting bearing faults. However, the existing bearing health indicators do not provide a reliable estimation of the fault characteristics, such as fault size and fault location. As a result, the ability to assess the severity of the bearing damage and to make maintenance decisions is limited.

The presented study is a part of an ongoing research on bearing prognostics, aimed to improve the understanding of the effects of fault size on the bearing dynamics. The research methodology combines dynamic modeling of the faulty bearing with experimental validation and confirmation of model simulations.

In the presented study, small faults (starting from 0.3 mm), simulating incipient damage are generated at increasing sizes by an electrical discharge machine. The recorded vibration data is then analyzed and compared to the vibration signatures predicted by the model. The experimental and the simulation results add new insights on the manifestation of the size of the fault and possible indicators of the damage severity.

1. INTRODUCTION

The ability to assess the bearing condition and to estimate its remaining useful life (RUL) is a key factor for machinery prognostics.

Our study is focused on estimating the position and size of the fault, based on the vibration analysis of the bearing. This study continues a former research that was conducted in BGU PHM lab aimed to find indications in the vibration signature of the size of the fault (Kogan, Shaharabany, Itzhak, Bortman & Klein, 2013). In the current study, we seeded groove shaped faults, of width between 0.3 and 1.2 mm into the outer-race of the bearing, which simulates realistic faults that often can be found in damaged bearings.

A 3D dynamic model (Kogan, Bortman, Kushnirsky, & Klein, 2012) was used to simulate faults and to study the effects of fault size and location on the vibration signatures. The analysis of the simulations results supported the interpretation of the experimental results.

This research was done in continuation to previous studies in order to improve the fault size estimation (Elforjani & Mba, (2010) and Sawalhi & Randall, (2011)).

2. EXPERIMENT DESCRIPTION

The experimental system includes two subsystems: a generic test rig (as shown in Fig.1) and a measurement unit. The generic test rig includes an AC motor, one shaft with two flywheels on it, mounted on two bearings.

The measurement unit includes a data acquisition system that is connected to an optic sensor and an accelerometer, the optic sensor measures the rotating speed of the shaft, and the accelerometer measures the vibration signals in three directions and is placed on the tested bearing housing (the right bearing in Fig 1).

Each test run was started with shaft alignment. The shaft speed was measured using Keyence optic sensor and vibrations were measured using a Dytran 3263A2 tri-axial

accelerometer. The data was acquired during 60 seconds with a sample rate of 25000 $\left[\frac{sample}{sec}\right]$.

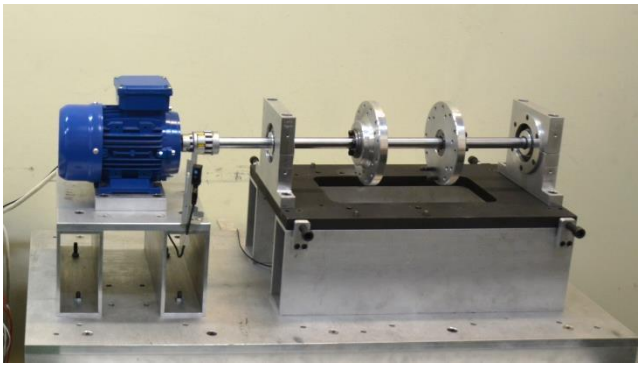

Figure 1. The test rig.

Six different bearings were monitored, a healthy bearing and five others with different fault sizes. Each bearing has been monitored in two fault locations, inside and outside the loading zone. The different fault locations were monitored in order to learn about the influence of the load applied on the fault.

2.1. Test configuration notation

The code of test runs includes 2 variables - the bearing number (noting the fault size) and the location of the fault. For example – "4B" is a bearing with a 0.61[mm] fault size, located 90° to the center of its loading zone. Table 2 summarizes the bearing parameters.

Table 1. Test configuration notation

Bearing number	Fault size [mm]	Location A loading zone	Location B $\mathbf{90^0}$ to the center of the loading zone
1	0	1A	-
2	0.31	2A	2B
3	0.39	3A	3B
4	0.61	4A	4B
5	0.78	5A	5B
6	1.12	6A	6B

Table 2. Bearing properties

Inner diameter	40[mm]
Outer diameter	80[mm]
Width	18[mm]
No. of balls	9
FTF	0.4X
BSF	2.4X
BPFO	3.6X
BPFI	5.4X

3. FAULT GENERATION PROCESS

In order to analyze the vibration signature of faulty bearings, we decided to use bearings that can be disassembled and reassembled without damaging any of the bearing parts during the process.

SKF ETN9 bearings having a "snap" type cage (see Figure 2) that can be removed from the bearing without damage.

Figure 2: SKF ETN9 "snap" type cage

After the bearing disassembly a fault was introduced in the outer ring using an EDM machine with customized copper electrodes (see Figure 3). The faults are thin groove shaped in various widths (see table 1).

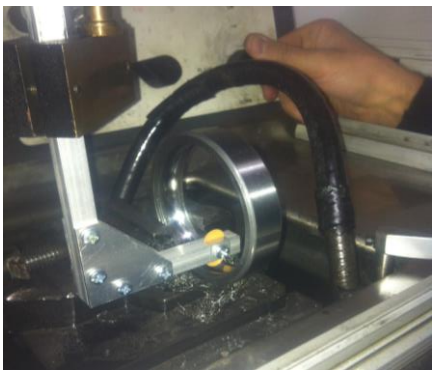

Figure 3: Bearing's outer race in the EDM process

Figure 4: Outer race with a groove shaped fault

4. MODEL DESCRIPTION

A 3D dynamic ball bearing model was developed to study the effect of faults on the bearing dynamic behavior. The aim of the model is to calculate the dynamic response of a bearing with a wide spectrum of faults. The algorithm was implemented numerically in MATLAB.

The dynamics, for each bearings component, are based on the classical dynamic equations

$$\Sigma\overrightarrow{F_f} + \Sigma\overrightarrow{F_n} = m\vec{a},\ \Sigma\left(\vec{R} \times \overrightarrow{F_f}\right) = \boldsymbol{I}\dot{\vec{\omega}}_{xyz} + \vec{\Omega} \times (\boldsymbol{I}\vec{\omega}) \quad (1)$$

where F_f, F_n are respectively the friction and the normal forces that act on a body, with mass m and acceleration $\vec{a}$; and $\Sigma\left(\vec{R} \times \overrightarrow{F_f}\right)$ is the total moment of force acting on a body with a moment of inertia tensor $\boldsymbol{I}$, angular velocity $\vec{\omega}$; body system xyz, with angular velocity $\vec{\Omega}$; and rotational acceleration, within the body system, $\dot{\vec{\omega}}_{xyz}$.

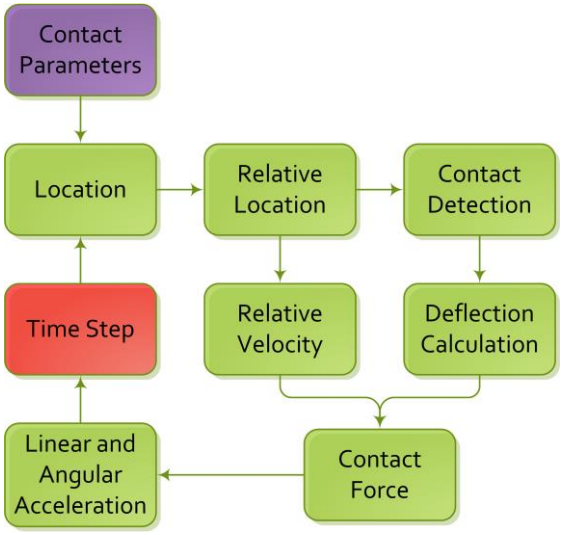

Figure 5. Simplified model algorithm

The relative velocity equation

$$\overrightarrow{v_b} = \overrightarrow{v_a} + \vec{\omega} \times \overrightarrow{ab} \quad (2)$$

Where $\overrightarrow{v_x}$ is the velocity of the body at $\vec{x}$ and $\vec{\omega}$ is the angular velocity of $\overrightarrow{ab}$.

The presented equations describe the motion of all the modeled bodies and are solved using time steps (see Fig. 5). In each time step, the solution of the equations is based on the previous time step solution, assuming a constant acceleration.

The dynamic model was validated by comparison to analytical solutions and known bearing response to local defects (Kogan, Bortman, Kushnirsky & Klein, 2012).

5. DATA ANALYSIS

The analysis process is similar for both the data acquired from the experiments and from the model, and it is described in figure 6. The resampled data rate is 2048 samples/cycle. The envelope of the acceleration data is calculated without filtering and the order domain of the envelope is achieved by calculating the 'Power Spectral Density' of the data, using 32 frames, which gives a resolution of 0.0156 order.

Figure 6: Data analysis process for the experiments and for the model data.

Since the model is simulating the acceleration on the bearings outer race without considering the transmission function to the sensor, we compared the order representation of the simulated data envelope and the order representation of the experimental data envelope. The order of the envelope reflects mainly the effects of the bearing filtering out most of the irrelevant data such as the transmission function and the effects of other rotating components.

Due to the simplicity of the test rig the bearings are the source for the vast majority of the peaks expected in the order of the envelope .Therefor, RMS of the order representation of the envelope is expected to provide a reliable indicator for the fault size. The RMS was calculated up to the 25th order and includes the first six BPFO harmonics and their sidebands.

The RMS level of the envelope of each of the runs was calculated. Then mean RMS value of each test configuration was calculated, average of three runs in similar conditions. Consequently, each configuration of the system (in each direction) is represented in the relevant graphs by a single mean value RMS.

6. RESULTS

6.1. Envelope spectrum

The fault pattern in the envelope spectrum is expected to contain peaks at the ball pass frequency over the outer race (BPFO) as well as lower sidebands caused by modulation of the shaft speed (McFadden & Smith, (1984)). Sidebands are expected due to imperfections of the test system such as unbalance and misalignment. Therefore, unbalance and normal radial clearance where simulated in the model.

The pattern was confirmed in the envelope order spectra of the test runs with faulty bearings and in the order spectra of the model. An example of an order spectrum of the envelope of bearing 1A (fault size 0.31 mm in the loading zone) is shown in Figures 7. Figure 8 contains the envelope order spectrum for the same fault size and location, as analyzed from the vibration signature of the experiment. In both

figures the BPFO, at order 3.6, and its harmonics are dominant, and numerous sidebands corresponding to the shaft speed can also be observed. It should be noted that the sidebands are lower by 2 degrees of order compared to the BPFO harmonics.

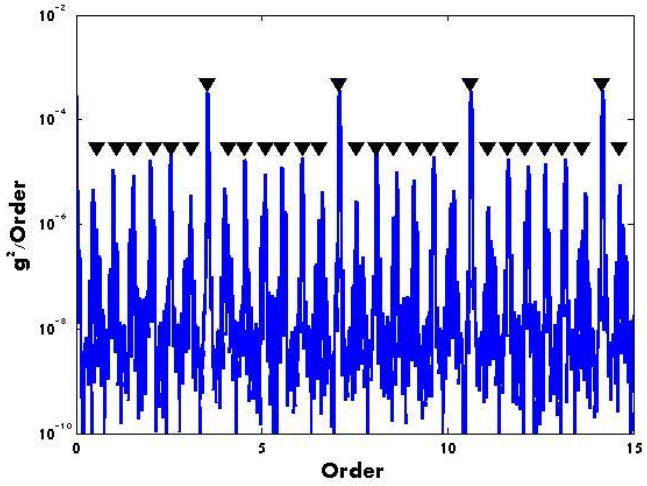

Figure 7. Model based results: order representation of the envelope of bearing with a 0.31mm fault located at the center of the loading zone. The triangles mark the BPFO harmonics and the related sidebands.

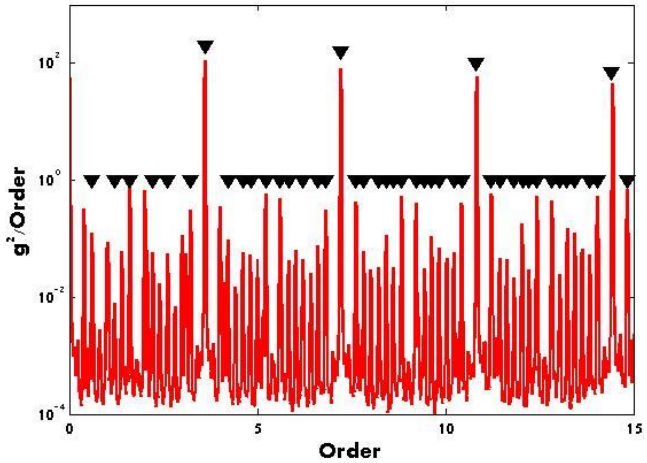

Figure 8. Experimental results: order representation of the envelope of bearing with a 0.31mm fault located at the center of the loading zone. The triangles mark the BPFO harmonics and the related sidebands.

It is notable that both the data from the experiments and from the model have the same general pattern.

6.2. Fault size and location – model

The model results, RMS levels of the envelope up to the 25th order as a function of fault size, are displayed in Figures 9 and 10. As can be seen in Figure 9, the RMS level of the envelope increases with the fault size. The RMS levels in the vertical direction of a fault located in the loading zone is significantly higher compared to the horizontal acceleration because the impulse generated by a ball passing the faulty surface is in the vertical direction. When the fault is located at 90^o to the center of the loading zone small forces (Sawalhi & Randall, (2008)) are applied in the vertical direction and the RMS levels remain constant.

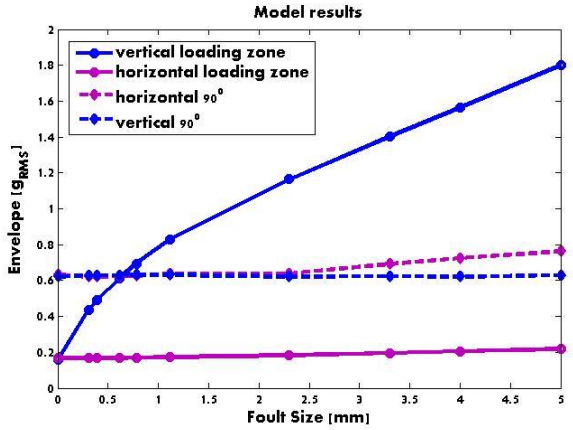

Figure 9. Model based results: RMS levels of envelope acceleration as a function of the fault size.

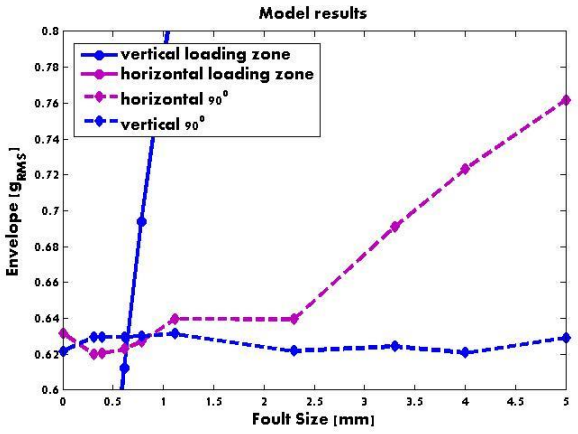

Figure 10. Model based results: RMS levels of envelope acceleration magnified to emphasize the prediction of a fault located at 90°.

It can also be observed that when the fault is located at 90^o , the RMS levels for faults above 2mm, in the horizontal direction are higher than the RMS levels in the vertical direction. The same conclusion was found in a former research (Kogan, Shaharabany, Itzhak, Bortman & Klein, 2013). The behavior of RMS levels for faults located at 90°, as predicted by the model, can be better observed in Figure 10, magnified in the appropriate range. For small size faults, up to 0.78mm the RMS levels are in the same range, whereas for bearings with larger faults, the RMS levels in the

horizontal direction are indeed getting higher compared to the RMS levels in the vertical direction (see Figure 10).

According to the results, it seems that the method proposed in Kogan, et al, 2013, which suggests to use the ratio between the horizontal and the vertical RMS as an indicator of the fault location is not applicable for small faults.

Since the model calculates the accelerations at the location of the fault in the outer race, the RMS levels differ for bearings without faults. In general, the levels of the vibrations at the different locations are not comparable.

6.3. Fault size and location – experimental results

The experimental results, RMS levels of the envelope up to the 25th order as a function of fault size, are displayed in Figures 11 and 12. In general, the trend of RMS level of the envelope corresponds to the defect size both in the horizontal and vertical directions. In addition, as seen in Figure 11, when the fault is located at the center of the loading zone, the envelope RMS levels in the vertical direction are higher than the RMS levels in the horizontal direction, as predicted by the model.

When the fault is located outside the loading zone at 90^o, the RMS levels in the horizontal direction are in the same range as in the vertical direction (see Figure 12). It can also be noted that the RMS levels in the horizontal direction are slightly lower than the RMS levels in the vertical direction, except for the bearing with fault size 1.12mm, as predicted by the model.

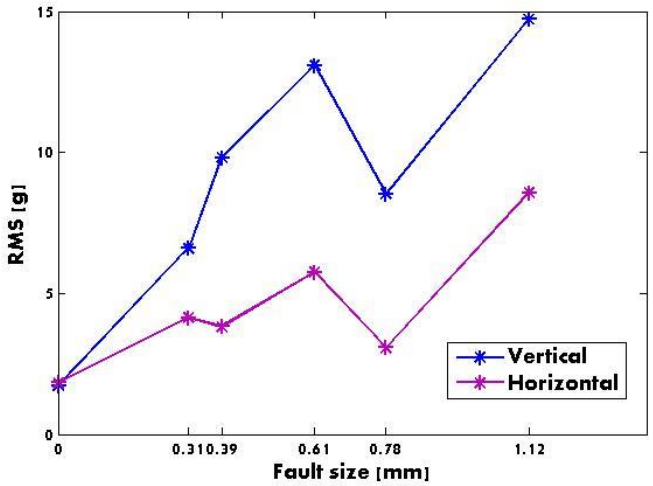

Figure 11. Experimental based results: RMS levels of envelope acceleration as a function of the fault size when fault located at the center of the loading zone (location "A").

When the fault is at the center of the loading zone, the runs with fault size 0.78mm seems to be out of the general trend. It was found that the background level of the relevant tests was extremely low compared to the other tests (up to three decades lower). The reason for this might be the initial alignment of the test kit, since shaft modulation is a result of unbalance and misalignment. Another explanation for the difference in the background level might be a slightly different structure of this particular bearing compared to the other defected bearings.

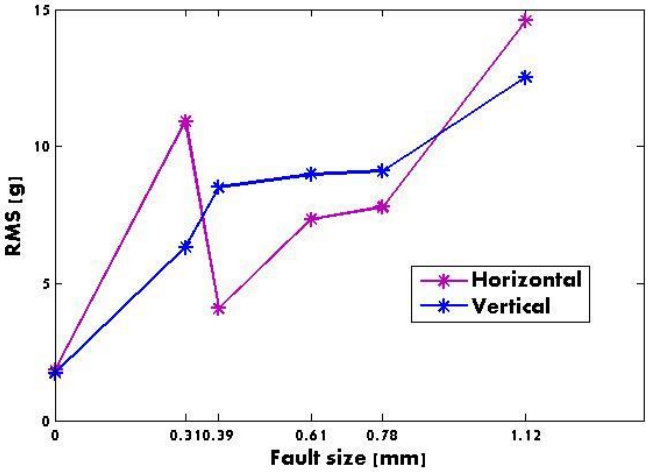

Figure 12. Experimental results of acceleration RMS vs fault size when fault located 90^o to the loading zone (location "B").

6.4. Experiments and model results comparison

The general pattern of the RMS levels as a function of fault size and location is similar in the model and the experiments. Generally, the RMS levels increase as the fault size increases, and the relations between the horizontal and the vertical RMS levels are similar.

RMS levels of the experimental results for a fault in and out of the loading zone were in the same range. However, the model shows a big difference in the RMS levels between the two locations. The reason for the difference is the transfer function from the fault to the sensor, which is not taken into consideration in the model simulations. Moreover, in the model the RMS levels represent the acceleration at two different locations on the outer race. In the experiments, both fault locations are measured at the same location on the bearing housing. The transmission paths from the two locations on the outer race to the sensor differ in the ranges of vibration levels.

7. CONCLUSIONS

A 3D ball bearing dynamical model was compared to test rig experiments in several fault sizes and locations. It was found that the behavior of the acceleration RMS levels as a function of the fault size are similar in the experimental and the model results. In both cases, the general RMS level increases. In addition, a new insight was found about the relation between

the vertical and the horizontal vibration levels as function of fault size and fault location.

It was found that the model provides a good prediction about trends and pattern of localized faults. This fact allows us continue the study of the effects of fault size and location using the model.

NOMENCLATURE

F	Force
I	Moment of inertia
R	Location vector
a	Acceleration
m	Mass
$\mathbf{v}$	Velocity
Ω	Body system angular velocity
$\boldsymbol{\omega}$	Angular velocity

REFERENCES

Sawalhi, N., & Randall, R. B. (2008). *Semi-automated bearing diagnostics – three case studies.* School of Mechanical and Manufacturing Engineering. The University of New South Wales, Sydney, Australia.

McFadden, P. D., & Smith, J. D. (1984). *Vibration Monitoring of rolling element bearing by the high-frequency resonance technique - a review*, Tribology international, Vol. 17, pp 3-10.

M. Elforjani, D. Mba. (2010). *Accelerated natural fault diagnosis in slow speed bearings with Acoustic Emission*. Engineering Fracture Mechanics 77 (2010) 112–127.

N. Sawalhi, R.B. Randall. (2011). *Vibration response of spalled rolling element bearings: Observations, simulations and signal processing techniques to track the spall size*. Mechanical Systems and Signal Processing 25 (2011) 846–870

Kogan, G., Bortman, J., Kushnirsky, A., & Klein, R. (2012). *Ball bearing modeling for faults simulation*, Ninth International Conference on Condition Monitoring and Machinery Failure Prevention Technologies, no. 1, pp. 1–8.

Kogan G., Shaharabany S., Itzhak I., Bortman J. & Klein R., (2013). *Towards Model Based Prognostics - Characterization of Fault Size in Bearings*, Annual Conference of the PHM Society 2013.